JOURNAL OF AIRCRAFT
Vol. 41, No. 4, July–August 2004

Reynolds-Averaged Navier–Stokes Simulations of Airfoils and Wings with Ice Shapes

Jianping Pan* and Eric Loth†
University of Illinois at Urbana—Champaign, Urbana, Illinois 61801-2935

Numerical simulations using the Reynolds-averaged Navier–Stokes equations were conducted to investigate the effect of simulated ridge and leading-edge ice shapes on the aerodynamic performance of airfoils and wings. A range of Reynolds numbers and Mach numbers, as well as ice-shape sizes and ice-shape locations, were examined for the NACA 23012, the NLF 0414, and the NACA 3415 airfoils. The results were compared to experiments completed recently at NASA Langley and University of Illinois. Additional two thinner airfoil models and a tapered NACA 23012 wing were also studied to investigate ice-shape location effect for various geometries. Comparisons between simulation results and experimental force data showed favorable comparison up to the stall conditions, with improved fidelity for forward and smaller ice shapes. At and past stall condition strong separation occurs, and the aerodynamic forces were typically not predicted accurately for large upper-surface ice shapes. To alleviate this problem, a lift-break (pseudostall) condition was defined based on the lift-curve slope change. The lift break compared reasonably well with experimental stall conditions and indicated that the upper-surface critical ice-shape location tended to be near (and often in between) the location of minimum pressure and the location of the most adverse pressure gradient.

Introduction

AIRCRAFT aerodynamic degradation caused by ice accretion is a severe problem faced by pilots and is thought to be responsible for many accidents. Ice accretion shapes can form at different locations on the aerodynamic surfaces under different meteorology and flight conditions. For example, ridge ice (which forms a spanwise ridge shape on the upper surface) can form when the deicing system is activated, and water droplets impinge forming ice accretion after the active portion of deicing system. Rime and glaze ice tend to respectively form round and horned protrusions near the leading edge. Those ice accretions can severely deteriorate the airfoil's aerodynamic performance.[1]

The effect of ice accretion on aerodynamics has been experimentally and numerically studied for many years, leading to a catalog of ice shapes and their effects for a variety of conditions. However, recent experiments by the University of Illinois' Icing Group employed a quarter-round shape on a NACA 23012 airfoil at the NASA Langley Low Turbulence Pressure Tunnel were the first measurements to systematically study Reynolds- and Mach-number effects of airfoils with ice shapes over a significant range of conditions. Additional measurements were obtained in the University of Illinois at Urbana—Champaign (UIUC) Low-Speed Wind Tunnel for the NACA 23012 and other airfoils for ridge ice shapes and leading-edge ice shapes, which further complement the preceding data set.[2–4]

Numerical simulations with Reynolds-averaged Navier–Stokes (RANS) method[5–9] have often shown trends similar to those obtained by experiments and as such can give guidance at other conditions. However, the complex flowfields associated with iced airfoils do not always allow robust predictions with conventional RANS methodologies, and a comprehensive numerical study on the RANS fidelity for a large variety of conditions has not been conducted. In particular, no numerical studies have investigated predictive performance in terms of Mach number and Reynolds number, as well as ice-shape size and location for a variety of airfoils. In addition, no computational studies have investigated the influence of ice-shape location on a wing three-dimensional geometry.

Taking advantage of the preceding recent experimental data set,[2–4] a parallel numerical investigation on ice-shape effect was conducted with two goals: 1) to provide a systematic view of the effect of ice accretion on airfoil and wing aerodynamics for various Reynolds numbers, Mach numbers, airfoil and wing geometries; and 2) to evaluate the fidelity of conventional RANS using a large range of experimental data and flow conditions. Additional details of the present study are available in a recent Federal Aviation Administration (FAA) report.[10]

Computational Methodology

The WIND 4.0 software package supported by the National Project for Application-Oriented Research in Computational Fluid Dynamics Alliance is used as the flow solver and for pre- and postprocessing. WIND is a structured, multizone, node-centered finite volume method solving the full compressible Reynolds-averaged Navier–Stokes equations with flexible turbulence models.[11]

Various one-equation and two-equation turbulence models were considered because the treatment of turbulent momentum transport is critical to the RANS flow predictions. In particular, selected iced airfoil cases were simulated with most popular turbulence models: the Spalart–Allmaras (S-A) one-equation model, the Baldwin–Barth (B-B) one-equation model, the shear-stress transportation (SST) two-equation model, and the k–ε two-equation model. The S-A model was chosen as the baseline turbulence model because of its good performance in the present comparisons and in previous studies.[5,6]

In this study transition points for the clean airfoil cases were based on the most upstream position of two locations: 1) the location of a trip strip (generally placed at 5% on lower surface and 2% on upper surface in experiments), and 2) the transition point location given by the integral boundary layer program of XFOIL.[12] For the iced airfoils the transition points were specified based on the most upstream position of three locations: 1) the location of a trip strip, 2) the transition point predicted for the counterpart clean airfoil at an equivalent lift, and 3) the ice-shape location.

Presented as Paper 2003-0729 at the Aerospace Sciences Meeting, Reno, NV, 8 January 2003; received 24 January 2003; revision received 30 June 2003; accepted for publication 30 June 2003.

*Graduate Research Assistant, Department of Aeronautical and Astronautical Engineering. Student Member AIAA.

†Professor, Department of Aeronautical and Astronautical Engineering, 306 Talbot Laboratory, 104 South Wright Street; loth@uiuc.edu. Member AIAA.

With respect to discretization, a single-block O-type grid is generated from the airfoil surface to 20 chords length away in all directions by using the grid-generator software.[13] The nondimensional first grid spacing in the normal direction is set as 2×10^{-6}, consistent with a y^+ of about one for all flow conditions. Based on grid-resolution studies (presented in the next section), the baseline grid include 400 points distributed along the airfoil surface (with about 100 points along the ice shape) and 100 points assigned in the normal direction. The grid distribution is clustered in the region where high flowfield gradients are expected, such as the leading-edge, trailing-edge, and ice-shape locations. For the simulations of the NACA 0012 and NACA 23012 wings, a total of 37 spanwise grid points was employed. A typical computational grid for an iced airfoil and surface grid for a tapered iced wing are shown in Fig. 1.

For the simulations included herein, a Roe second-order upwind scheme (specialized for stretched grids) is selected to discretize the convection terms on the right-hand side of the equations. This scheme was chosen because it was considered the most robust scheme with favorable accuracy of those available in WIND. The steady-state solution was generally obtained with a local Courant–Friedrichs–Lewy (CFL) number of 1.3 to ensure the numerical stability as well as to accelerate the convergence. Only fully converged RANS results are presented, where convergence was recorded when the norm residue reaches a level 10^{-6} or lower. The computations were completed on both National Center for Supercomputing Applications SGI Origin 2000 workstation and UIUC Turing Linux Cluster Systems. Each simulation took approximately 2 s of CPU time per cycle and approximately 12,000 cycles for convergence.

Methodology Validation

Grid-Independence Study

To evaluate the grid sensitivity and optimization, the WIND code was first validated for a clean NACA 23012 airfoil at the baseline NASA Langley low turbulence pressure tunnel (LTPT) experimental condition of $M = 0.12$ and $Re = 10.5 \times 10^6$. In total, four grids (300×100, 400×100, 400×50, 400×200) were tested for this validation case. Figures 2a and 2b show the lift-curve distributions, drag, and pitching-moment coefficient distributions for the clean NACA 23012 airfoil with different grid resolutions as well as the experimental LTPT results.[4] In general, the aerodynamic coefficients were well predicted for all of the grids (except for the 400×50 grid, which is not shown). In particular, increasing the grid points along the streamwise direction from 300 to 400 or increasing the grid points in the normal direction from 100 and 200 yielded no significant difference.

To ensure that a 400×100 resolution was also generally sufficient for iced airfoils, a particularly challenging ice-shape condition was chosen for the grid-resolution test. Figures 2c and 2d show the lift, drag, and pitching-moment coefficients for a typical iced airfoil with $x/c = 0.10$, $k/c = 1.39\%$ ice shape on the NACA 23012 airfoil. No significant difference was found for the simulation results based on the 400×100 and the 600×200 grids. As such, the 400×100 grid was deemed to provide grid-independent results and was chosen as the baseline grid in all of the simulation cases to keep the balance of the accuracy and computer resource.

Turbulence Model Selection and Lift-Break Definition

As already noted, three representative and commonly used models (B-B, S-A, and SST) were selected to evaluate their capability, and all three gave good predictions for clean airfoils. Predictions for a particularly challenging upper-surface ice shape in terms of lift, drag, and pitching moment are shown in Fig. 3. As seen in the figures, the B-B model generally does not provide as good results as the other two models. Results based on the S-A and SST models are close to each other for the drag and moment predictions. However up to the experimental stall angle, the lift predicted with the S-A model is more representative of the experimental data. This is also consistent with a previous turbulence model survey conducted with an unstructured grid flow solver for iced airfoils.[6] In addition, as a one-equation model the S-A model generally takes less time to converge as compared to the two-equation SST model. Therefore, the S-A model was herein selected as the baseline turbulence model in this study.

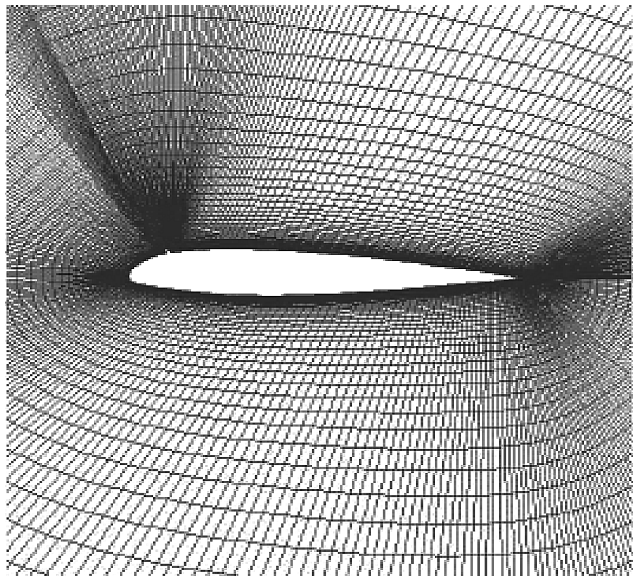

a) Far-field view for airfoil

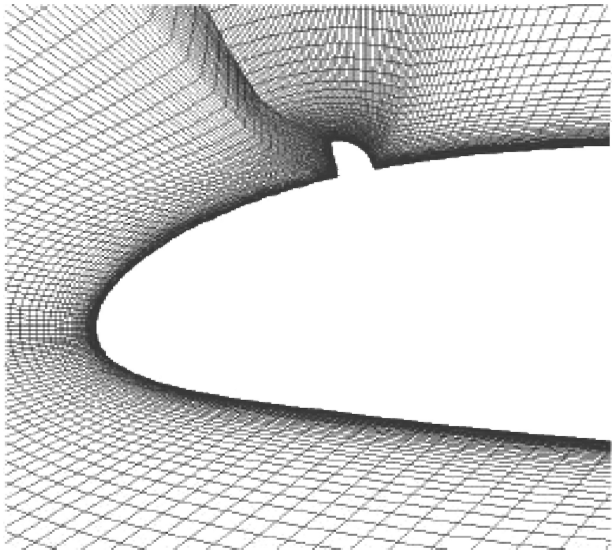

b) Close-up view for airfoil

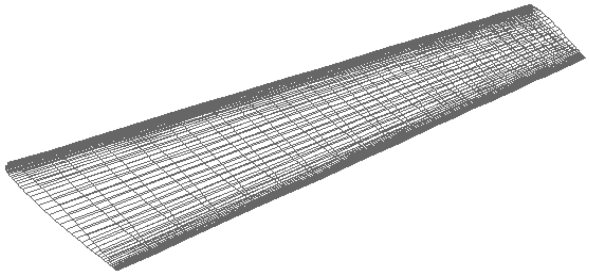

c) Surface grid for tapered wing

Fig. 1 Computational grid for iced NACA 23012 airfoil and tapered wing.

However, in this particular example there is no obvious maximum lift coefficient and stall subsequent behavior for any of the simulations, even though the experimental data shows these two aspects. This is attributed to the inability of the RANS technique to correctly predict the rapidly growing nonlinear recirculation bubble aft the ice shape, especially at higher angles of attack when this bubble dominates the upper-surface distribution.[5] At these conditions the entire

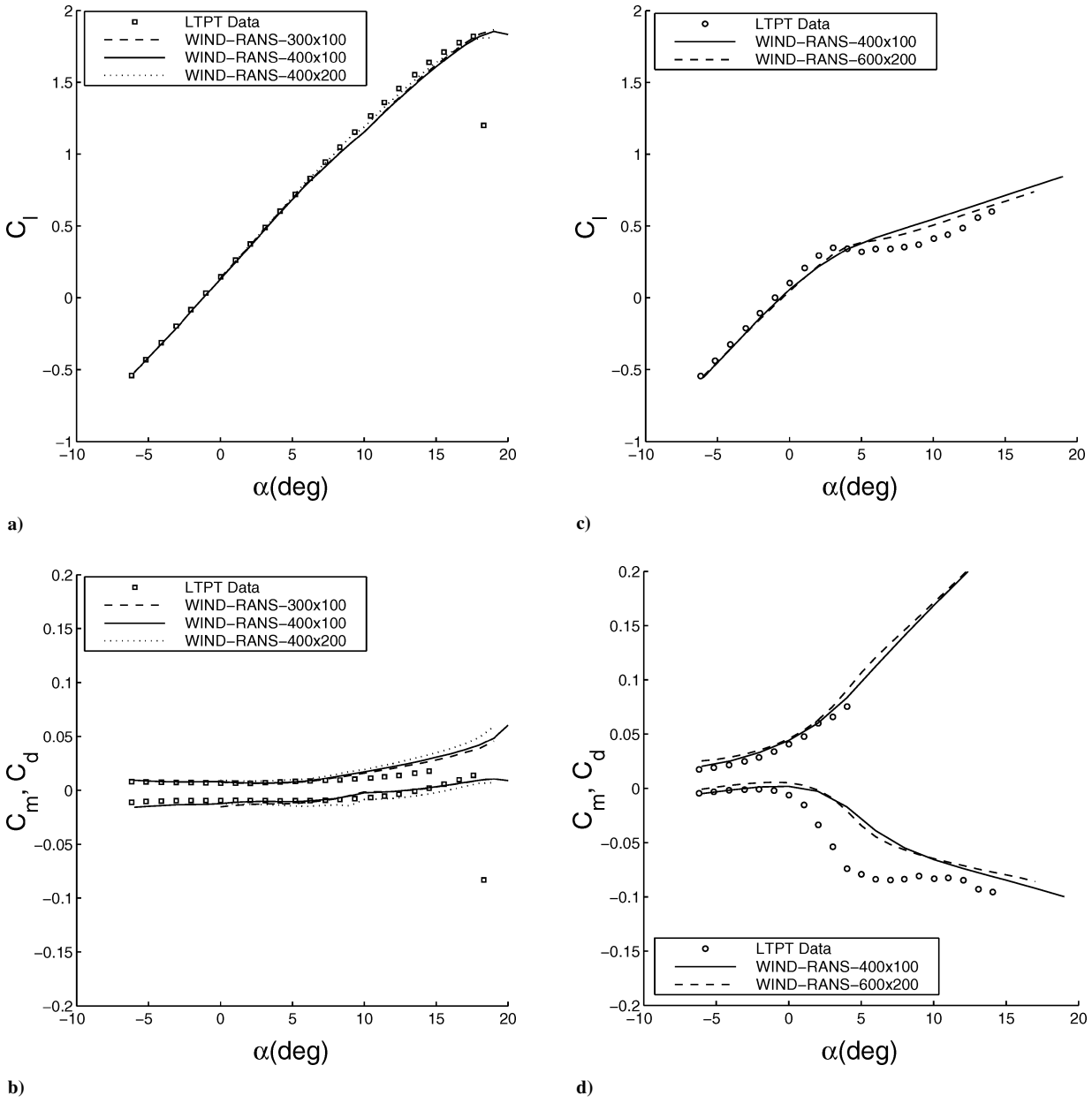

Fig. 2 Lift, drag, and pitching moment for NACA 23012 airfoil ($k/c = 1.39\%$, $x/c = 0.10$) at $Re = 10.5 \times 10^6$, $M = 0.12$ with various grid resolutions: a, b) clean airfoil and c, d) iced airfoil.

separated region becomes highly unsteady even prior to stall,[14] and the steady-state RANS prediction approach appears unsuitable to adequately predict the entrainment rate within the separated flow region and the subsequent downstream boundary-layer recovery.

Because the RANS approach cannot predict a maximum lift coefficient for some large ice-shape configurations, a pseudostall condition (based on the break of the lift curve) was defined herein and used to indicate the experimental stall conditions. To demonstrate this definition, Fig. 4 shows the lift curve slope at various angles of attack for the same conditions as Fig. 3. A significant change in the predicted lift-curve slope $C_{l\alpha}$ is noted, which occurs near the experimental stall angle of attack of 3.5 deg. This correlation was expected because the change in lift-curve slope is generally related to the rapidly growing flow separation and recirculation bubble on the upper surface predicted in RANS. Therefore, the lift-curve slope change can serve as the pseudostall condition. In this study a lift-break angle of attack α_{break} was defined as the angle of attack where $C_{l\alpha}$ is 50% of $C_{l\alpha,\max}$, where this maximum lift-curve slope occurs in the linear range at lower angles of attack (below 0 deg in this case). In this particular example the maximum $C_{l\alpha}$ at -2 deg is 0.106, so that $C_{l\alpha}$ at lift-break condition is 0.053 at 4.8 deg, and the corresponding lift-break coefficient ($C_{l,\text{break}}$) is 0.38.

Wing Validation

To assess ice location sensitivity for a wing, a three-dimensional validation for the WIND code was conducted for a rectangular NACA 0012 wing at $Re = 1.5 \times 10^6$ and $M = 0.12$ with both clean and leading-edge ice-shape conditions. The computational grid has a normal and streamwise resolution comparable with that of Kwon and Sankar,[9] although a finer spanwise resolution was included herein, that is, 37 vs 25 points. Also note that the Baldwin–Lomax one-equation model was applied in Kwon and Sankar's simulation, whereas the more robust S-A model was applied herein.

In corresponding to experimental results,[15] simulations were conducted at an angle of attack of 8 deg for the clean wing and at 4 deg and 8 deg for the iced wing. Figures 5a and 5b show the sectional C_l prediction at different spanwise locations for the clean and iced wings. For the clean wing the performance of the present simulation is reasonable (although there is a slight overprediction near the tip) and comparable to that of Kwon and Sankar's predictions.

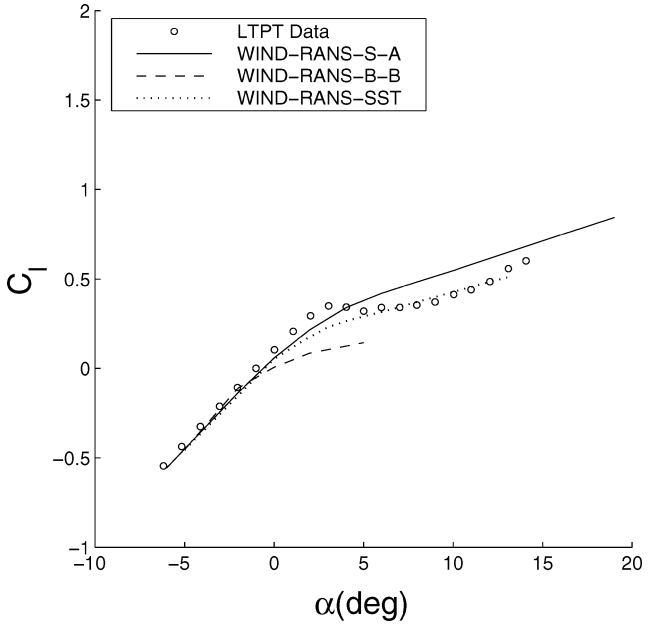

a) Lift

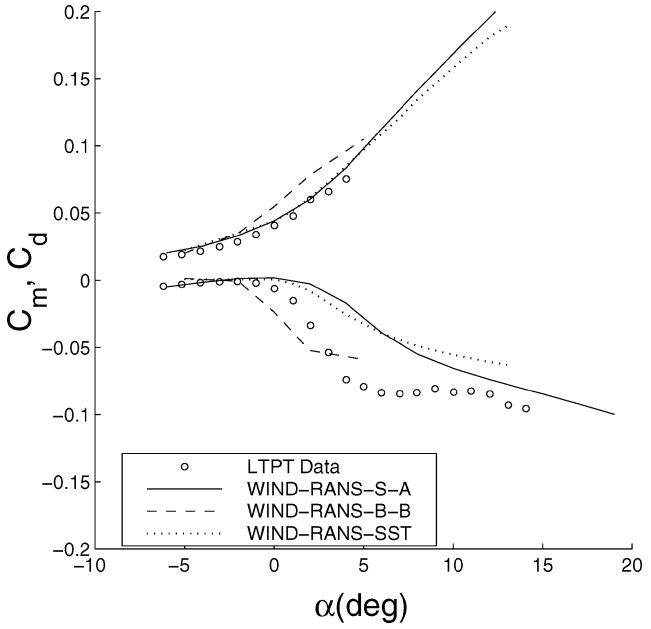

b) Drag and pitching moment

Fig. 3 Lift, drag, and pitching moment for iced NACA 23012 airfoil ($k/c = 1.39\%$, $x/c = 0.10$) at $Re = 10.5 \times 10^6$, $M = 0.12$ with various turbulence models.

For the iced wing at 4 deg, the predicted lift value represents the experimental data quite well. However, there is somewhat of an overprediction for the angle of attack of 8 deg (presumably because it is close to the stall angle of attack). Compared with Kwon and Sankar's simulation, the present predictions tend to have a better performance, especially for the section lift near the root plane at 8 deg. This might be a result of the increased spanwise grid resolution and the improved turbulence model. The pressure coefficient at the midspanwise is also compared in Figs. 5c and 5d. Again the agreement between WIND prediction and experimental data is quite good.

In summary, the WIND code with the S-A turbulence model reasonably predicted the section lift and pressure distribution for both clean and iced NACA 0012 wing configurations, and the approach can be considered reasonable for investigating effects of ice-shape location on wing aerodynamics, which will be presented in the later part of the results with a more realistic (e.g., tapered) wing.

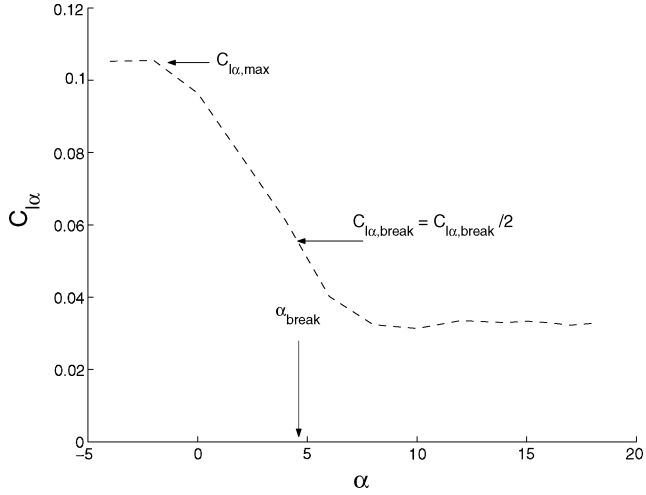

Fig. 4 Lift-curve slope and lift-break definition for iced NACA 23012 airfoil ($k/c = 1.39\%$, $x/c = 0.10$) using the S-A model.

Results and Discussion

Effect of Reynolds Number

Reynolds-number effects were studied for clean and iced NACA 23012 airfoils at a fixed Mach number 0.12. The results for Reynolds numbers of 3.5×10^6, 7.5×10^6, and 10.5×10^6 were compared with experimental data obtained in the NASA Langley LTPT wind tunnel in Fig. 6.

In general, the WIND predictions for the lift coefficients with different Reynolds numbers on a clean NACA 23012 airfoil exhibit good comparisons with the experimental data (Fig. 6a). However, the WIND lift-curve slope includes a slight break at about 5 deg, yielding small underpredictions of the lift for higher angles of attack. This can be attributed to the imprecisely predicted transition process. However, the maximum lift coefficient is well predicted, and stall angles of attack are predicted to within 2 deg. Both experimental and numerical results show that both lift coefficient and stall angle of attack increase somewhat with increasing Reynolds number from 3.5×10^6 to 10.5×10^6. This small change is attributed to a more upstream transition point at higher Reynolds number, which in turn transfers more turbulent energy into the boundary layer to delay the separation, and so increases the angle at which stall occurs.

As in the prediction of lift, a discrepancy in drag was predicted for angles of attack above 5 deg as shown in Fig. 6b. The qualitative trend of a modest decrease in drag coefficients with increasing Reynolds number was reasonably captured by WIND. The pitching-moment coefficients were also well predicted by WIND, where the coefficient minor increases show only with the increasing angle of attack until a drop-off at stall. Both the numerical predictions and the experimental results show a negligible difference of C_m as the Reynolds number was varied.

The effect of Reynolds number on an iced NACA 23012 airfoil is shown in Figs. 6c and 6d for a $k/c = 1.39\%$ quarter-round ice shape located at 10% chord. The experimental results show that the stall type changed from a leading-edge stall for the clean case to thin-airfoil stall for the iced case. However, as noticed before in Fig. 3, no obvious maximum lift coefficient and stall are predicted in the numerical results. As such, a lift-break condition was defined as in Fig. 4, yielding a lift-break angle of attack of 4.8 deg and a lift-break coefficient of 0.38, which are close to the experimental stall lift coefficient of 0.35 at 3 deg. The negligible sensitivity of lift to Reynolds number is found experimentally and computationally and is attributed to the flow separation being forced to take place at the ice-shape location, independent of upstream boundary-layer development.

The predicted drag coefficient (Fig. 6d) is independent on the variation of Reynolds number for the iced airfoils (whereas small decreases were noted in the clean-airfoil cases). The drag predictions agree well with experimental data before the lift-break angle of attack at about 5 deg (beyond which no experimental data were

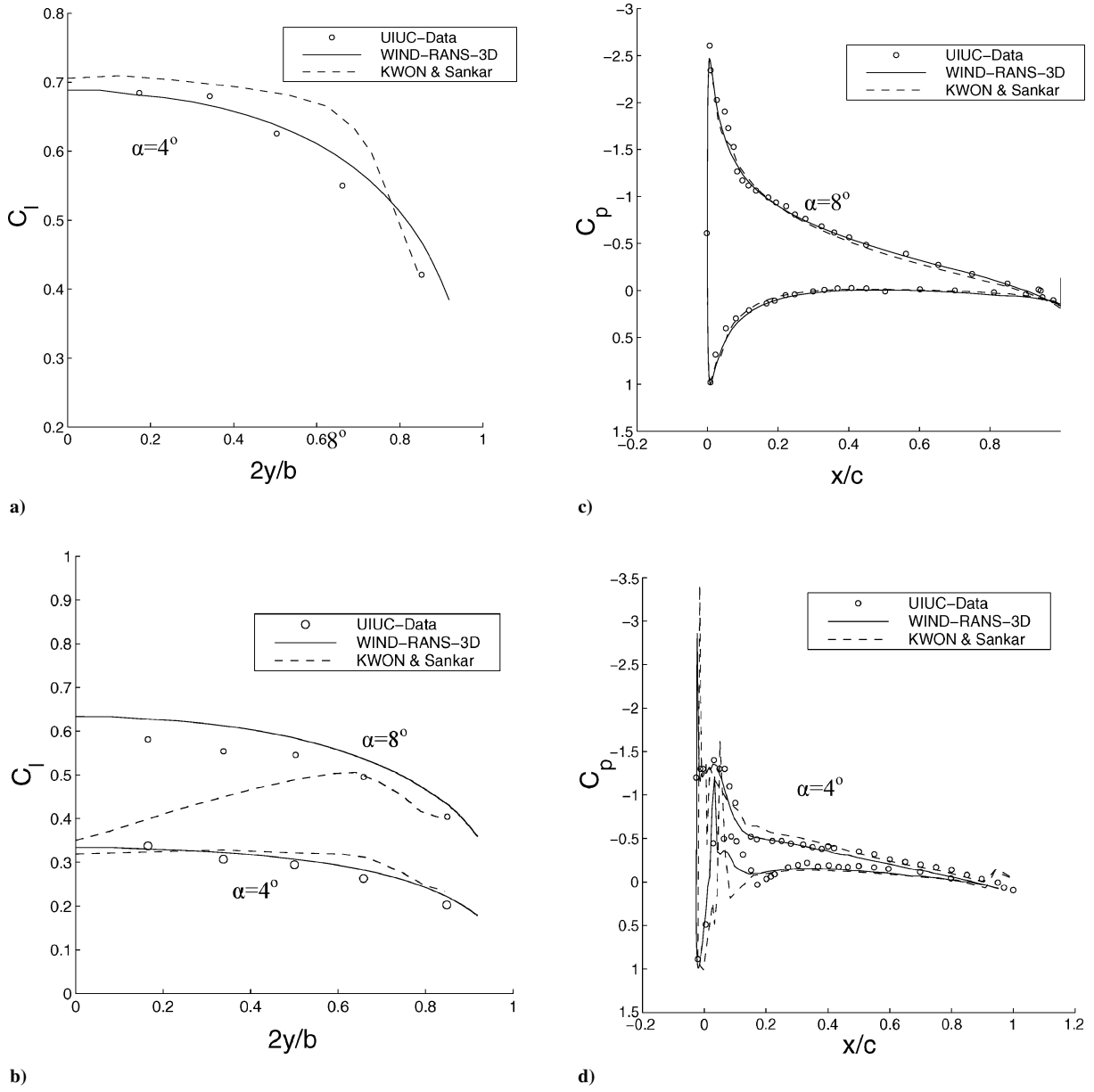

Fig. 5 Rectangular NACA 0012 wing simulation at $Re = 1.5 \times 10^6$, $M = 0.12$ showing the following: a) section lift at $\alpha = 8$ deg for clean wing as a function of spanwise location, b) section lift at $\alpha = 4$ and 8 deg for iced wing as a function of spanwise location, c) midspan pressure distribution at $\alpha = 8$ deg for clean wing, and d) midspan pressure distribution at $\alpha = 4$ deg for iced wing.

available). The effect of Reynolds number on the pitching moment is also negligible, both experimentally and computationally. A small increase of pitching moment can be found in both cases for negative angles of attack. However, for positive angles of attack the measurements yield a more rapid fall-off than the predictions. This is attributed to the inability to properly predict details of the pressure distribution associated with the separation bubble after ice-shape location (to be discussed later).

Effect of Mach Number

The effect of Mach number was examined for both clean and iced NACA 23012 airfoils, at the fixed Reynolds number at 10.5×10^6 with three different Mach numbers (0.12, 0.21, and 0.28) corresponding to the LTPT experimental conditions in Fig. 7. The trends of the lift-coefficient features are well predicted except for the consistent slight underprediction of lift-curve slope beyond 5 deg. With the increment of Mach number, both experimental and numerical results show a decrease in the maximum lift coefficients and angle of attack at which stall occurs. Although the slope of the lift curve increases with Mach-number increase at positive prestall angles of attack (consistent with the Prandtl–Glauert rule for compressibility effect), increased Mach number also reduces the stall angles of attack as it enlarges the laminar region and leads to an earlier separation. As found previously in the Reynolds-number study, the clean-airfoil drag (Fig. 7b) is somewhat overpredicted at higher positive angles of attack while the pitching moment is accurately predicted. The experimental drag and moment coefficients increase with the compressibility at positive angles of attack, which is consistent with the increment of lift-curve slope at this region, and the predictions.

Figures 7c and 7d show the compressibility effect on an NACA 23012 airfoil with same ice configuration investigated in Fig. 6. The results (experiments and predictions) show that the lift coefficients for Mach number 0.12 are slightly greater than those for Mach number 0.28, especially near the experiment stall (or lift-break) angle of attack. Although the experimental data show a thin-airfoil stall at 3-deg angle of attack, there is again a lack of an obvious stall in the simulations, although the lift-break angle of attack occurred about 5 deg.

For drag coefficients the compressibility effect is weak in both predictions and experiments (as compared to clean airfoils), and in

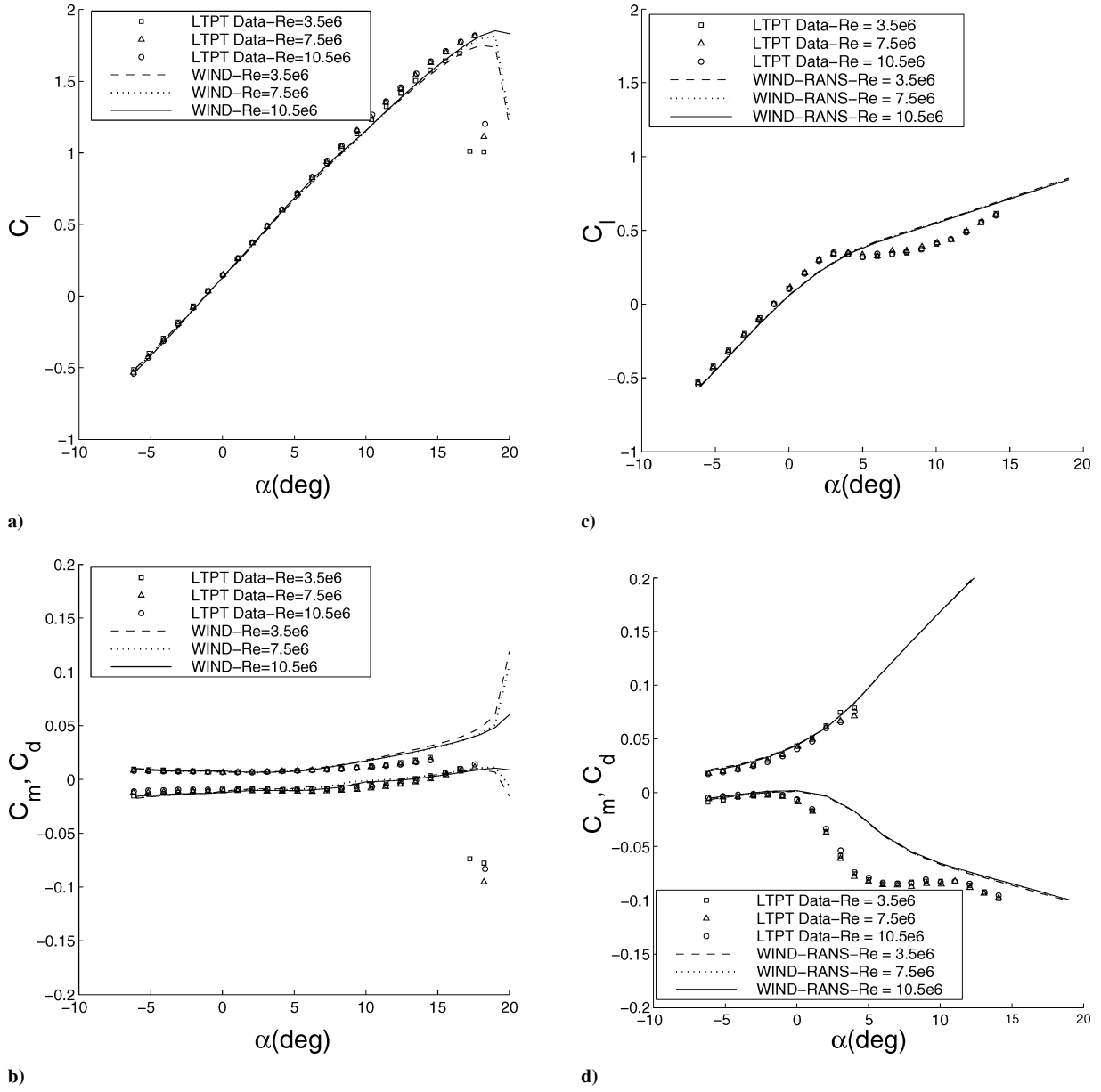

Fig. 6 Reynolds-number effect on lift, drag, and pitching moment for NACA 23012 airfoil ($k/c = 1.39\%$, $x/c = 0.10$) at $M = 0.12$: a, b) clean airfoil and c, d) iced airfoil.

general the drag is higher than in the clean case, and the predictions show good agreement (actually better than the clean case). A weak decrease in moment is found for an increasing compressibility effect, and again the experimental rapid reduction at 0 deg is only qualitatively predicted. In all cases similar comments regarding prediction fidelity as in Fig. 6d are also appropriate for the results shown in Fig. 7d. Therefore, the prediction fidelity is generally not a function of Reynolds number or of Mach number.

Effect of Ice-Shape Size

The effect of ice-shape size on aerodynamic performance was considered for the NACA 23012 airfoil and the NLF 0414 airfoil in Fig. 8. The NACA 23012 airfoil included an upper-surface quarter-round ice shape at $x/c = 0.10$ for $k/c = 0$, 0.83 and 1.39%, whereas the NLF 0414 includes a leading-edge horn ice shape at $s/c = 3.4\%$ for $k/c = 2.22$, 4.44, and 6.67%.

Figure 8a shows the effect of upper-surface ridge ice-shape size on the lift coefficient for the NACA 23012 airfoil at the LTPT experimental $Re = 10.5 \times 10^6$ and $M = 0.12$. The break of the lift-curve slope indicates that rapid changes in lift occur around 5 deg for $k/c = 1.39\%$ ice shape and around 6 deg for $k/c = 0.83\%$ ice shape. For the larger ice shape ($k/c = 1.39\%$) WIND gives reasonable predictions of the dramatic reductions in the stall/lift-break coefficient (from 1.82 to 0.35 experimentally and from 1.85 to 0.38 numerically) and stall/break angle of attack (from about 17.6 to 3.0 deg experimentally and from 19.0 to 4.8 deg numerically). For the smaller ice shape with a size 60% of the larger ice shape ($k/c = 0.83\%$), the lift-break coefficient was still dramatically low (0.55 numerically), and similarly, the break angle of attack was also quite low (6.2 deg numerically). This indicates a nonlinear reduction of lift and stall/break angle with changes in the magnitude of ice-shape size.

Figure 8b shows the drag and pitching-moment predictions. While at low angles of attack, both WIND and experiments yield a similar marked increase of drag with ice accretion size, especially at positive angles of attack. For the low angles of attack before stall, increment in the ice-shape size also increases the pitching-moment coefficient. However, for positive angles of attack of the ice-shape cases the pitching moment drops dramatically. The predicted trends also indicate a nonlinear change of C_d and C_m with respect to ice-shape size (k/c).

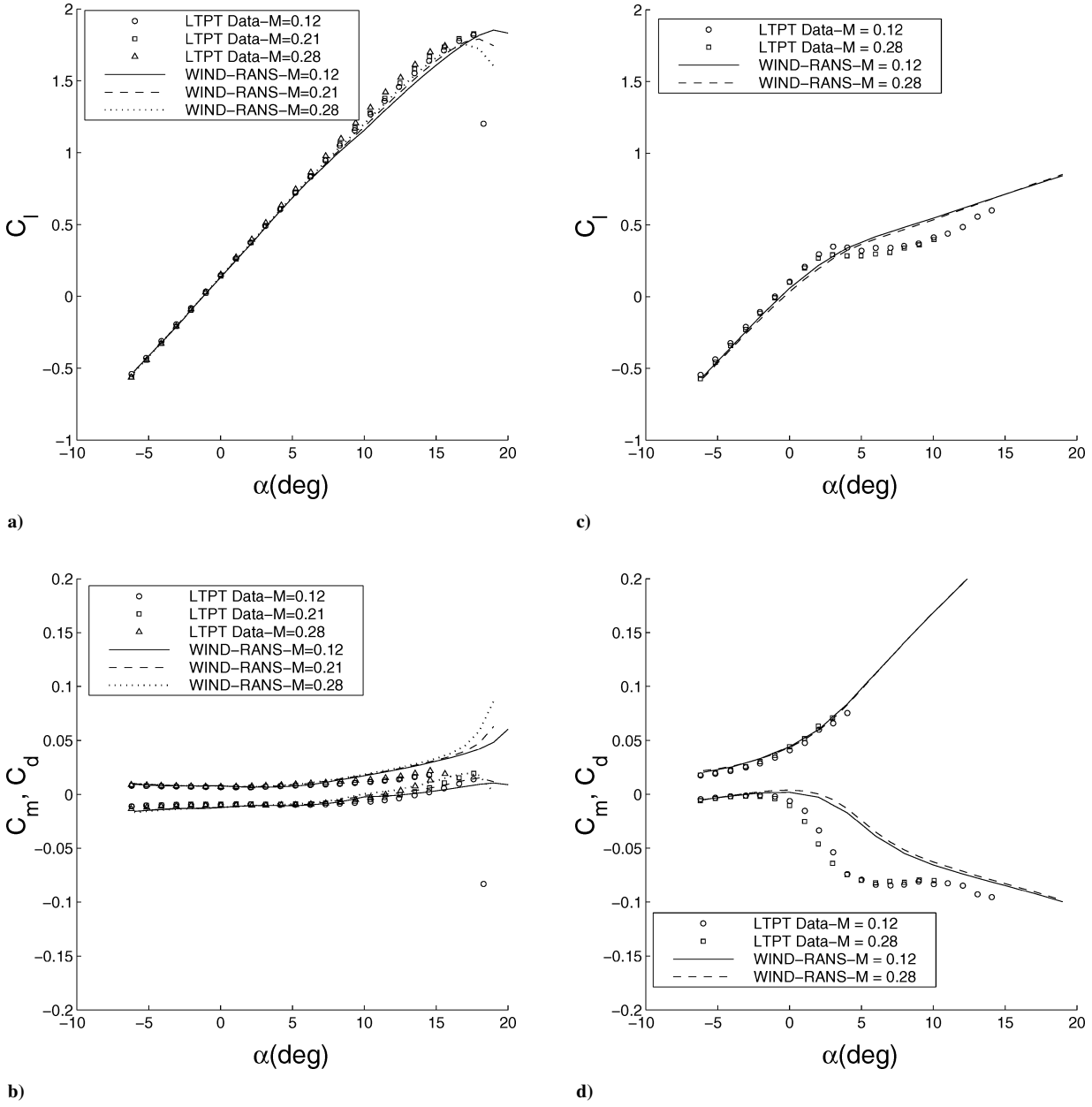

Fig. 7 Mach-number effect on lift, drag, and pitching moment for NACA 23012 airfoil ($k/c = 1.39\%$, $x/c = 0.10$) at $Re = 10.5 \times 10^6$: a, b) clean airfoil and c, d) iced airfoil.

The effects of leading-edge ice-shape size on the NLF 0414 airfoil are shown in Figs. 8c and 8d. A horn ice shape was attached to the NLF 0414 airfoil at a leading-edge location corresponding to $s/c = 3.4\%$ (a location close to $x/c = 0.02$). All cases were investigated at the UIUC experimental conditions of $Re = 1.8 \times 10^6$ and $M = 0.185$, consistent with the UIUC experimental study.[3] Figure 8c shows the lift predictions. With an increment of ice-shape size at this location, both the stall/break angle of attack and the maximum/lift-break coefficient decrease significantly. Note that the predictions do yield a $C_{l,\max}$ for the smallest ice-shape size but only yield a break in the lift-curve slope for the larger ice shapes. Therefore, the problem of predicting $C_{l,\max}$ is not as severe as for a typical upper-surface ice-shape location, but is still significant. Considering a maximum lift coefficient of 1.35 for the clean NLF 0414, the lift degradation is modest compared to the quarter-round ridge ice shapes. The predicted lift-break coefficients for the smallest ice shape ($k/c = 2.22\%$) drops to 0.71 at $\alpha = 5.4$ deg, while the measured $C_{l,\max}$ similarly drops to 0.72 at $\alpha = 5.1$ deg. The figure also shows that the leading-edge ice shapes tend to have a linear reduction with respect to change in ice-shape sizes.

At low angles of attack (< -5 deg), the difference for the drag is small, but large increases are noted experimentally and numerically at larger angles of attack for increasing ice-shape size (Fig. 8d). The predictions (and experiments) also indicate that higher pitching moments are associated with larger ice shapes at negative angles of attack (<0 deg), whereas the reverse is true at positive angles of attack up to stall. Notably, the largest pitching moment is found a few degrees in advance of stall/break angle of attack (which decreases with increasing ice-shape size). In general, Fig. 8 demonstrates that the lift (especially stall) and pitching-moment prediction fidelity is highest for the leading-edge ice shapes and for the small ice-shape sizes.

Effect of Ice-Shape Location

With the ice shape located at different positions, its effect on airfoil aerodynamics can vary significantly. At a "critical" ice-shape location the most deteriorated aerodynamics is obtained for a given ice-shape size. To investigate the ice-shape location effect, simulations were performed for the NACA 23012 airfoil and other airfoil models with ice shapes, as well as for a NACA 23012 wing.

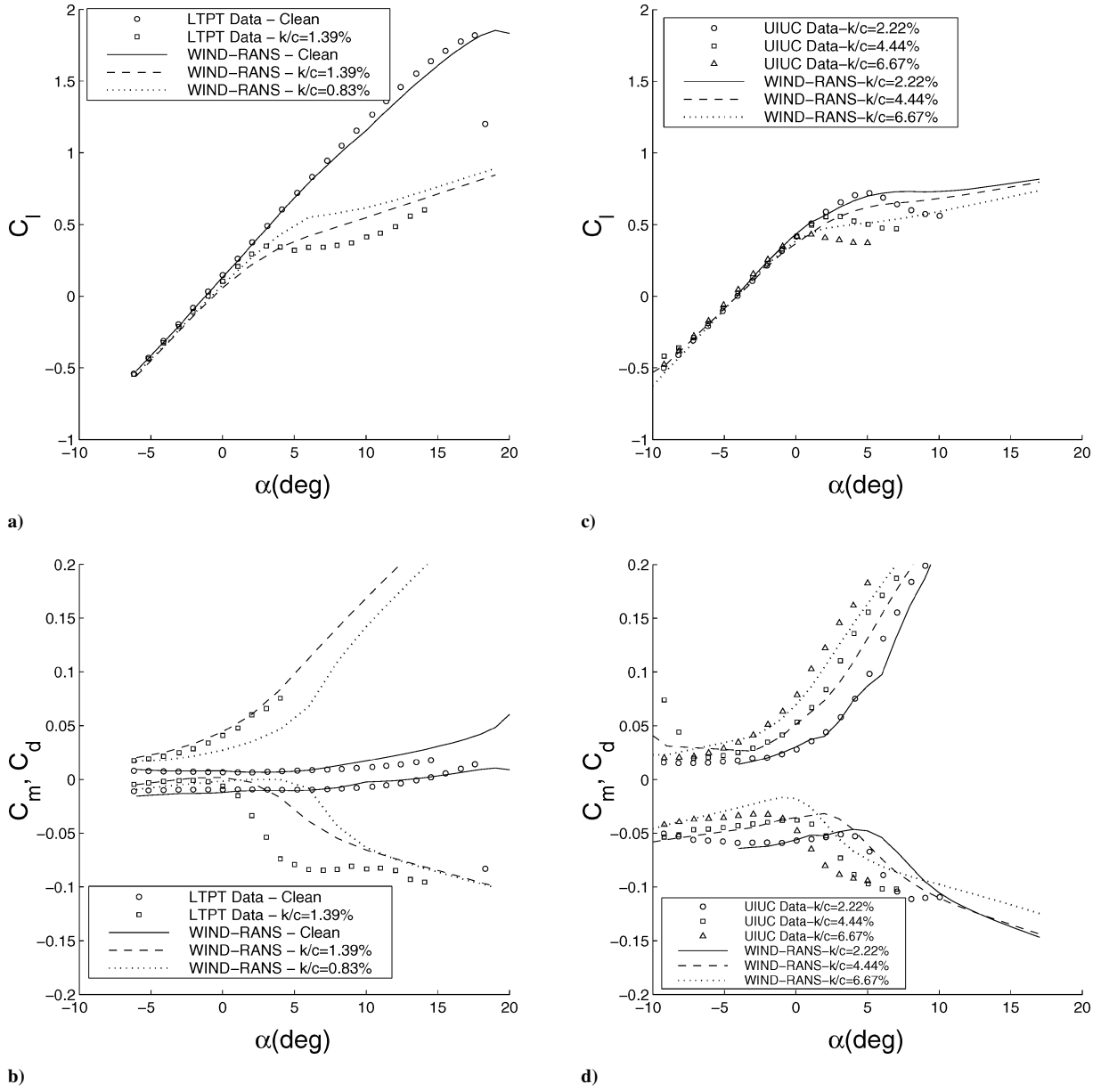

Fig. 8 Ice-shape size effect on lift, drag, and pitching moment for a, b) NACA 23012 iced airfoil ($x/c = 0.10$) at $Re = 10.5 \times 10^6$, $M = 0.12$; c, d) NLF 0414 iced airfoil ($s/c = 3.4\% \sim x/c = 0.02$) at $Re = 1.8 \times 10^6$, $M = 0.185$.

NACA 23012 Airfoil

The effect of ice-shape location on the lift, drag, and pitching-moment coefficient was studied for the NACA 23012 airfoil with both leading-edge and upper-surface ice-shape configurations (Fig. 9). For the upper-surface ice shapes a quarter-round ice shape with $k/c = 1.39\%$ was attached at different locations to be representative of the two-dimensional ridge ice; for the leading-edge ice shapes a horn ice shape with a larger $k/c = 4.4\%$ was attached at different locations to be representative of glaze ice-shape configurations. Simulations were performed at the LTPT condition of $Re = 10.5 \times 10^6$ and $M = 0.12$ to be comparable to LTPT experimental results.

In Fig. 9a the $k/c = 4.44\%$ horn ice shapes were studied at three leading-edge locations: $x/c = 0.0$, 0.95, and 1.9%. There is a less severe reduction (from the clean case) of the lift-curve slope and maximum lift coefficient for the ice shapes at the immediate leading-edge location $x/c = 0.0$. In particular, the maximum lift coefficient is reduced from 1.85 in the clean case to 1.08, and the predictions show a definite maximum lift coefficient (not just a break) at this location, though the drop-off is not as mild as was found experimentally. However, for the ice shape at $x/c = 0.95\%$ the lift-break coefficient drops more than two-fold (from 1.08 to 0.49). For the ice shape at $x/c = 1.9\%$, the penalty is even more severe as the $C_{l,\text{break}}$ drops to a lower value of 0.39. For the range considered herein, the most aft position ($x/c = 1.9\%$) is thus the most critical ice-shape location. During this investigation, the predicted results were important in identifying that the lift from the pressure taps neglected a significant force on the ice shape itself. The use of the force balance data showed a result more consistent with the predictions and here thus used.

Figure 9c shows the lift for a $k/c = 1.39\%$ quarter-round ice shape at three upper-surface positions of $x/c = 0.02$, 0.10, and 0.20. A thin airfoil stall was predicted in $x/c = 0.02$ case with a stall lift coefficient of 0.53. (This is another case in which a break value need not be defined.) For the $x/c = 0.10$ case a lower lift-break coefficient of 0.38 was predicted at about 5 deg (roughly compatible with the experimental value of 0.35 at $\alpha = 3$ deg). For $x/c = 0.20$ the lift-break coefficient is 0.52 and occurs at angle of attack about 7 deg. Thus, the largest reduction in the maximum/lift-break coefficient for three locations considered is for the $x/c = 0.10$ case. Considering that this reduction is larger than the $x/c = 0.02$ case (the most critical location of the leading-edge locations for an even larger ice shape),

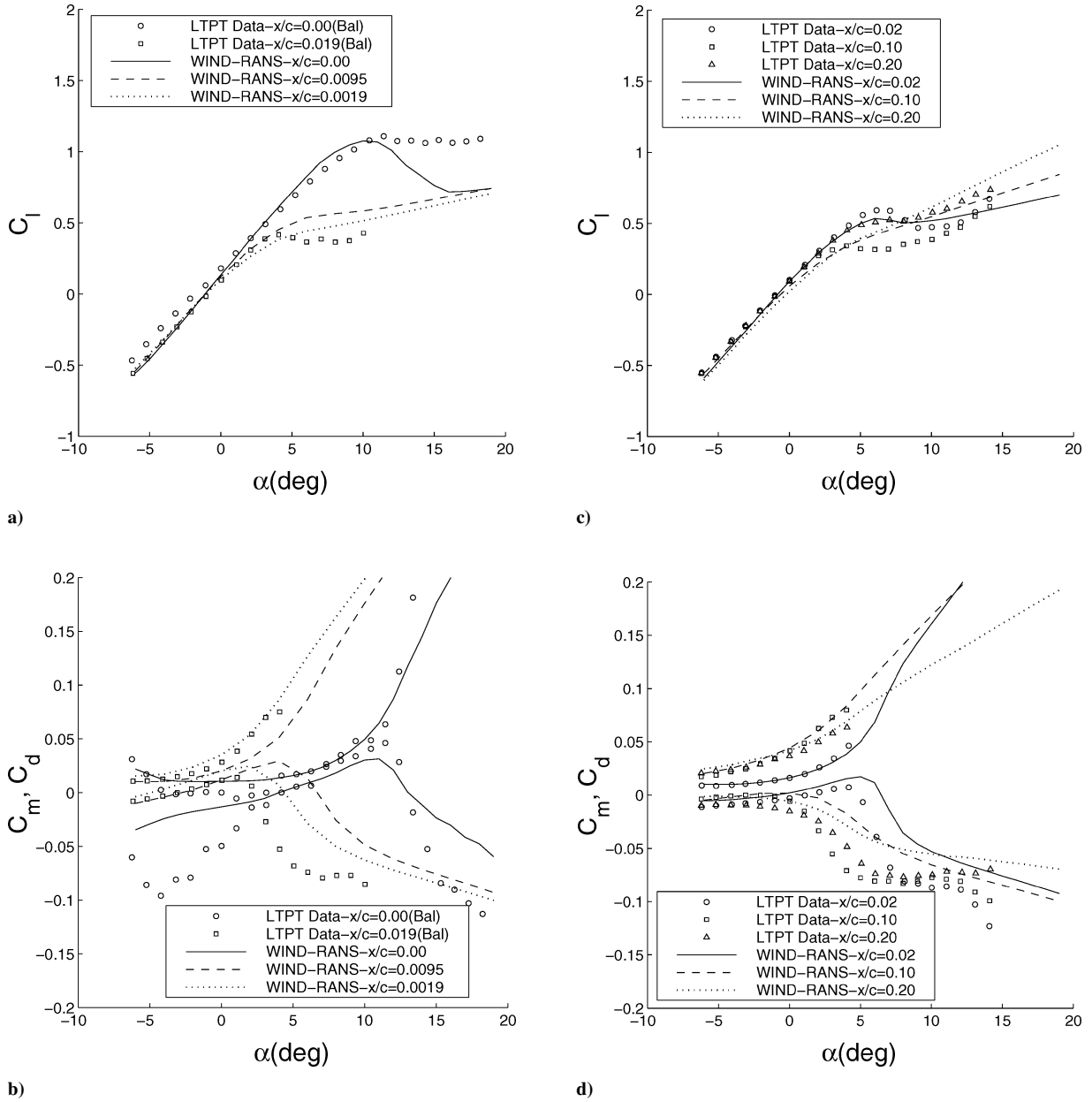

Fig. 9 Ice-shape location effect on lift, drag, and pitching moment for NACA 23012 airfoil at $Re = 10.5 \times 10^6$, $M = 0.12$: a, b) $k/c = 4.4\%$ horn ice shape at leading-edge locations and c, d) $k/c = 1.39\%$ quarter-round ice shape at upper-surface locations.

the $x/c = 0.10$ is deemed the predicted (and experimental) critical ice-shape location for the NACA 23012 airfoil.

As shown in Fig. 9b, the drag increased as the ice-shape location moved downstream from $x/c = 0.0$ to 1.9% for the leading-edge ice shapes at positive angles of attack. For the upper-surface ice-shape cases the largest drag was predicted and measured for $x/c = 0.10$ cases at the positive angles of attack (Fig. 9d), which demonstrates that the most deteriorated aerodynamics takes place with the ice shape at this location (once a fixed size is considered).

For the pitching moment of the leading-edge ice-shape cases (Fig. 9b), the negative angles of attack yield increases as the ice shape is located more downstream. At positive angles of attack, the reverse trend is found, and the tendency to drop-off is exacerbated as the ice location move aft to 1.9%. At negative angles of attack, the $x/c = 0.0$ ice-shape location yielded very low values of C_m that were not quantitatively predicted. This is attributed to problems in predicting a lower-surface ice-shape induced separation bubble. For the upper-surface ice-shape cases (Fig. 9d) the $x/c = 0.10$ for the ice-shape location yields the earliest drop-off of the pitching moment (with respect to increasing angle of attack), which is consistent with its poor lift and drag performance. Again, the numerical performance tended to improve with ice shapes located near the leading edge and with the smaller ice shapes (e.g., a definite stall was predicted at the most upstream of the 4.4% ice shapes and at the most upstream condition of the 1.39% ice shapes).

The pressure distributions and streamline profiles at 0 deg for the upper-surface ice-shape cases are shown in Fig. 10. In general, the pressure is well predicted for the lower surface and upper surface in front of ice shape, which is consistent with excellent prediction of clean airfoil C_p distribution. After the ice shape the extent of the separation region is not well captured, especially with the $x/c = 0.10$ simulation case. Note that the separation bubble length for $x/c = 0.20$ is 22% of the chord, whereas for $x/c = 0.10$ it is 23% of the chord, such that bubble separation length can be a predictor of critical ice-shape location, but the sensitivity is weak. However, both the experiments and predictions show that the $x/c = 0.10$ case indicates the largest change in the pressure coefficient over the ice shape, which suggests that the upstream C_p distribution might be more important.

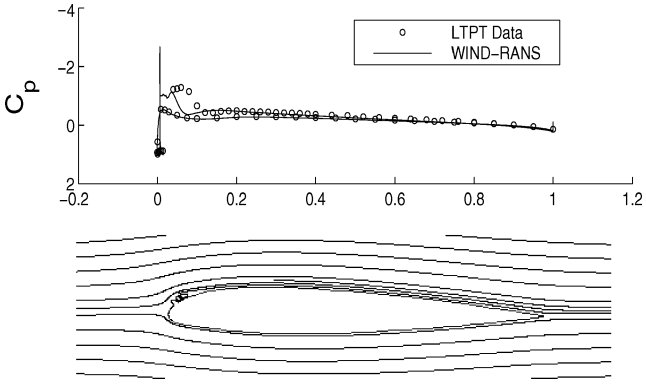

a) $x/c = 0.02$

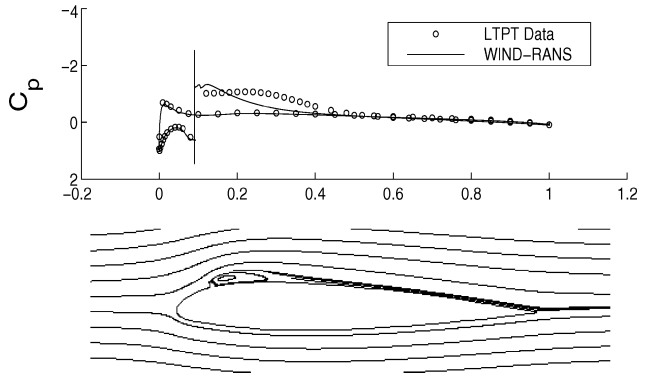

b) $x/c = 0.10$

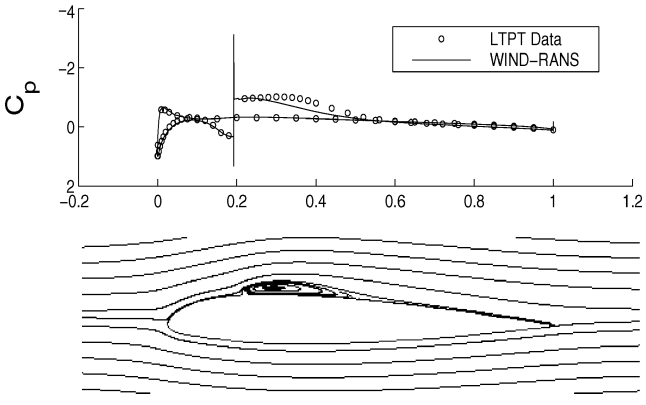

c) $x/c = 0.20$

Fig. 10 Pressure distributions and streamlines for the upper-surface iced NACA 23012 airfoil at $\alpha = 0$ deg, $Re = 10.5 \times 10^6$, $M = 0.12$.

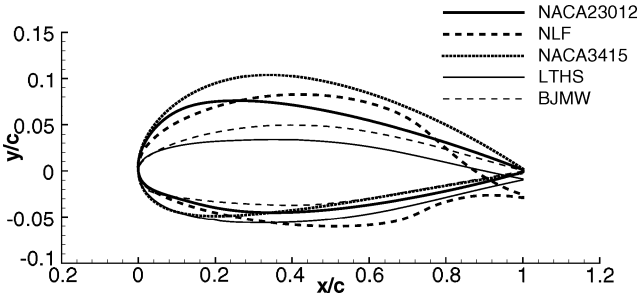

a)

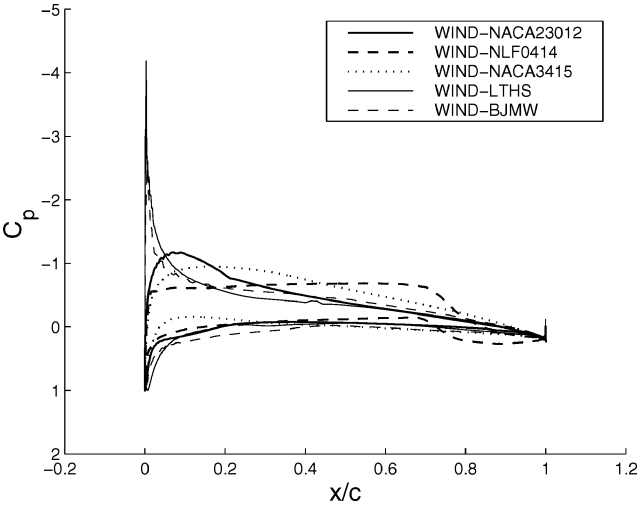

b)

Fig. 11 Five clean airfoils: NACA 23012, NLF 0414, NACA 3415, LTHS, and BJMW showing the following: a) geometry configurations and b) pressure distributions at $C_l = 0.5$.

Other Airfoils

The effect of ice-shape location was also studied for four other airfoils: NACA 3415, NLF 0414, large transportation horizontal stabilizer (LTHS), and business-jet main wing (BJMW). Each included the same forward quarter-round ice shape ($k/c = 1.39\%$) attached at different upper-surface or leading-edge locations. The clean geometries and pressure distributions (at $C_l = 0.5$) of these four airfoils and the NACA 23012 airfoil are shown in Fig. 11. A much more front-located pressure suction peak is evident for the two thinner airfoils, the LTHS and the BJMW, whereas the NLF 0414 airfoil yielded no distinct pressure peak location.

Figure 12 shows the lift curves for each airfoil in the clean status and with ice shapes attached at different locations. Whereas the lift slope for the clean NACA 3415 and NLF 0414 airfoils were somewhat overpredicted for positive angles of attack, the lift coefficients are reasonably predicted up to stall angle of attack for all of the iced cases (and beyond stall for the $x/c = 0.02$ condition). The critical ice shape for the NACA 3415 airfoil was found at $x/c = 0.20$ with a lift-break angle 4.5 deg and lift-break coefficient value of 0.43. This is similar to the experimental critical ice shape at $x/c = 0.20$ with stall angle of 4.0 deg at a $C_{l,\max}$ of 0.32. For the NLF 0414 airfoil (experimentally and computationally) the critical ice shape moves downstream further at $x/c = 0.30$, with a predicted lift-break angle of 3.4 deg and lift-break coefficient value of 0.51 (similar to the experimental stall angle of 5.0 deg at a $C_{l,\max}$ of 0.58). In general, the lift is much less sensitive to x/c location for the NLF 0414 airfoil as compared to that of the NACA 3415 and NACA 23012 airfoils. This is consistent with the stronger variation of C_p along the chord for the latter two airfoils. The LTHS and BJMW airfoils were found to have a much more upstream critical ice-shape location as $x/c = 0.01$ was found to yield the most deteriorated aerodynamics. This can be expected as these two airfoils are much more front loaded, that is, their C_p peak is near the leading edge.

The relation between the predicted stall/lift-break coefficients and the ice-shape locations for different airfoils is shown in Fig. 13a along with experimental stall values. All of the airfoils showed strong degradation such that the stall/break C_l values were all in the range of 0.3 to 0.6. Therefore, the most deteriorated aerodynamic performance occurred when ice shapes were located at 10% for the NACA 23012, 20% for the NACA 3415, and 30% for the NLF 0414, respectively. Note that the NACA 23012 did not produce a distinct lift break at $x/c = 0.3$, the NACA 3415 did not produce a converged solution for $x/c = 0.3$, the experimental stall occurred sooner at $x/c = 0.2$ than at $x/c = 0.3$, and the NLF 0414 did not produce a clear $C_{l,\text{stall}}$ or $C_{l,\text{break}}$ at $x/c = 0.5$. The two other airfoils, LTHS and BJMW, have a more forward critical ice-shape location at about 1% of chord length. Thus the thicker airfoils were more sensitive to upper-surface ice shapes, whereas thinner airfoils were more sensitive to leading-edge ice shapes.

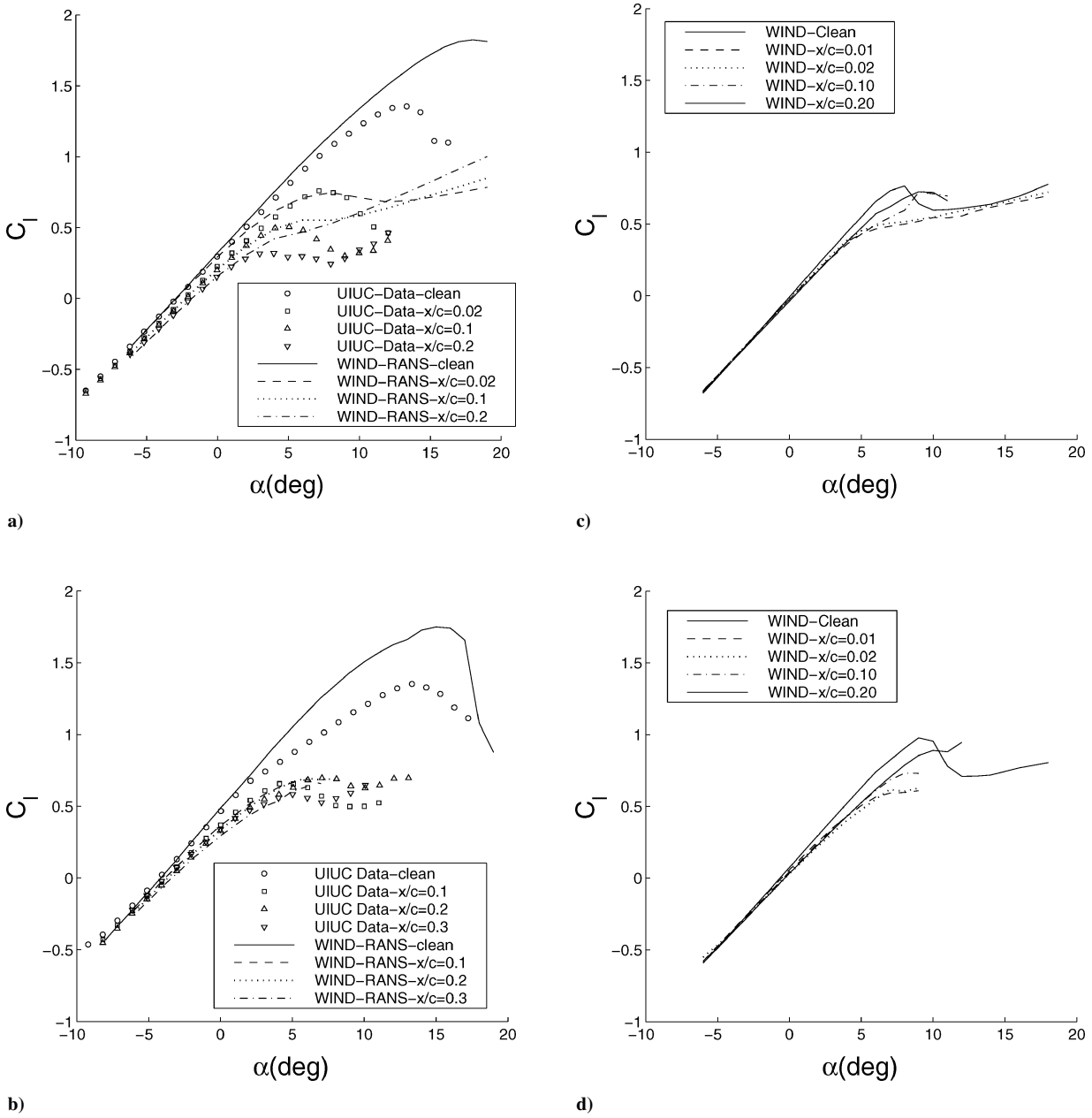

Fig. 12 Ice-shape location effect ($k/c = 1.39\%$) on lift coefficient for a) NACA 3415, b) NLF 0414, c) LTHS, and d) BJMW.

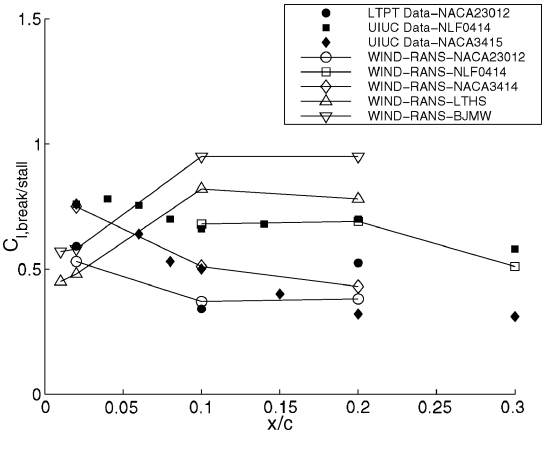

Fig. 13a Ice-shape location effect on stall/lift-break coefficient for the iced airfoils.

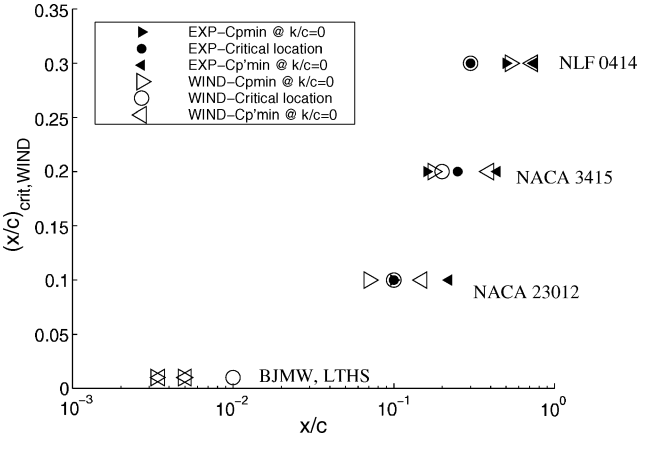

Fig. 13b Relation between critical ice-shape locations and their clean airfoil minimum pressure and minimum pressure gradient locations at $C_l = 0.5$.

The significantly different aerodynamic responses to the ice shapes for those airfoils can be related to the different aerodynamic load patterns in their clean models. As seen in Fig. 11b, the suction peaks of the two thinner airfoils, the LTHS and the BJMW, are quite close to the leading edge. For the NACA 23012 airfoil the suction peak is located at around 7% of the chord length. And for the NACA 3415 airfoil, its at about 18% of chord length. There is a suction peak for the NLF 0414 airfoil about 50% of chord, but the C_p distribution includes a nearly flat plateau ranging from 5% to the 65% chord location. Lee and Bragg[2] suggested that the measured critical ice shape generally occurs between the locations of $C_{p,\min}$ (pressure suction peak) and $C'_{p,\min}$ (most adverse pressure gradient, i.e., where $-\mathrm{d}p/\mathrm{d}x$ is greatest) of the clean airfoil case at a C_l value of 0.5. This can be correlated to the fluid physics whereby one might expect that an ice shape at the highest velocity around the airfoil (at the $C_{p,\min}$) would be detrimental, but also an ice shape at the most adverse pressure gradient (at the $C'_{p,\min}$) could be critical as well. Figure 13b shows the relation between the critical ice-shape locations and their clean airfoil $C_{p,\min}$ and $C'_{p,\min}$ locations (corresponding to $C_l = 0.5$) for both measurements and predictions. The critical ice shape is in between the clean $C_{p,\min}$ and $C'_{p,\min}$ locations for the NACA 23012 and the NACA 3415, but it is not necessarily true for the NLF 0414 (where the C_p peak is given as a range). For the LTHS and the BJMW the critical ice-shape location tends to be aft of both the $C_{p,\min}$ and $C'_{p,\min}$ locations, but by a margin of less than 1% of chord length. Therefore, the critical ice shape is generally in the neighborhood of the clean $C_{p,\min}$ and $C'_{p,\min}$ locations (but not necessarily in between them). Finally, the numerical predictions of all of these locations is quite reasonable once the lift-break definition is employed.

It is of interest to determine whether the aerodynamic deterioration (in terms of either the magnitude of the stall/lift-break coefficient or percent reduction from the clean value) is correlated with the magnitude of the $C_{p,\min}$ for the clean case. With the largest clean airfoil $C_{p,\min}$ among the thick airfoils, the NACA 23012 airfoil yields the largest lift reduction (80%) at the critical ice-shape location. However, the NLF 0414 still has a 70% lift reduction although it has a much smaller $C_{p,\min}$. In addition the NACA 3415 yields the lowest overall stall/lift-break coefficient. Among the thin airfoils (which have very high pressure peaks as compared to the other airfoils) the performance degradation is not as significant, and in particular the BJMW airfoil is the least affected. Therefore,

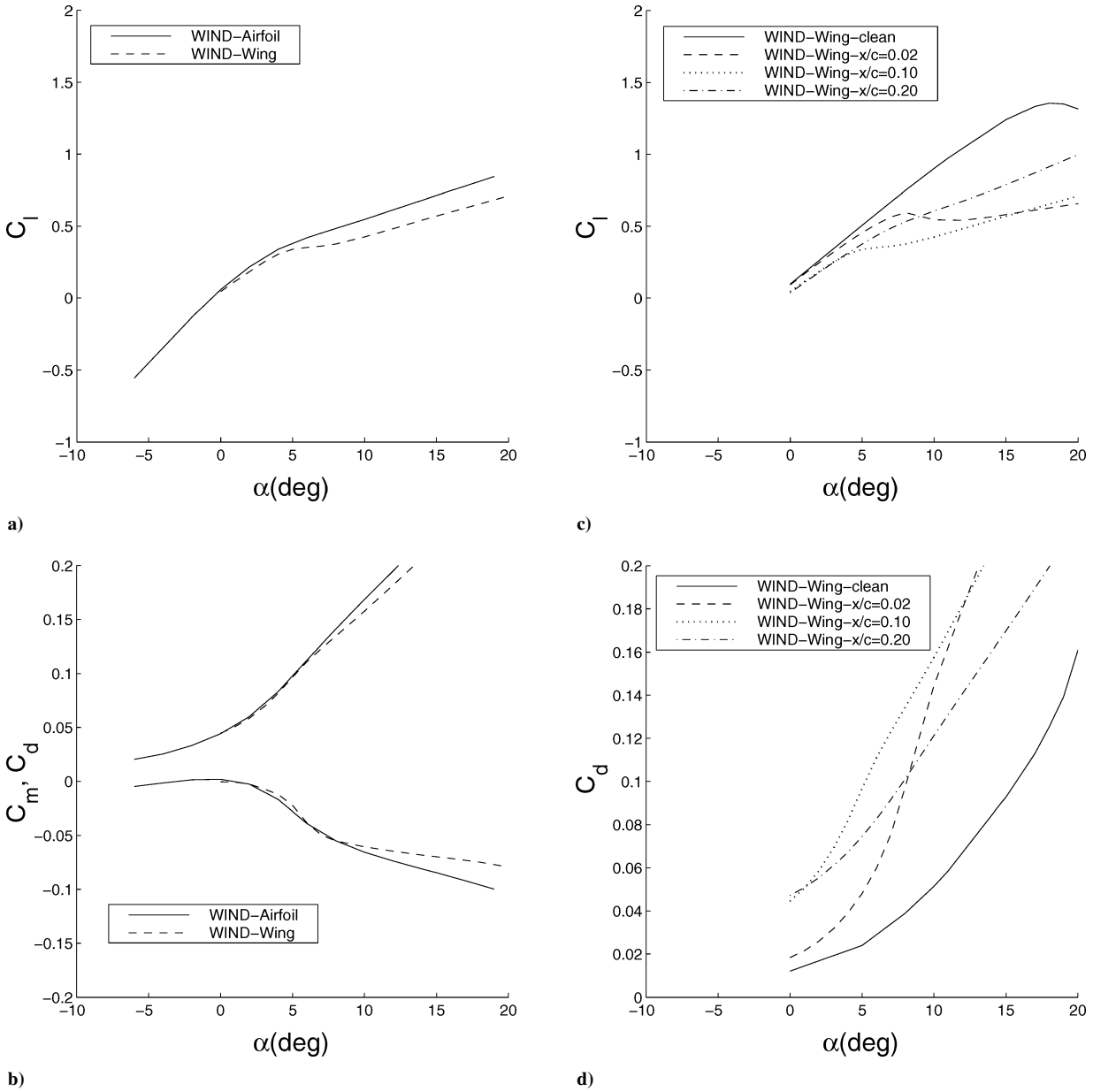

Fig. 14 Simulations for a NACA 23012 wing ($k/c = 1.39\%$) at $Re = 10.5 \times 10^6$, $M = 0.12$: a, b) comparisons with two-dimensional airfoil lift and drag ($x/c = 0.10$) and c, d) ice-shape location effect on wing lift and drag coefficients.

the clean airfoil C_p magnitudes do not strongly correlate with the reduction with either the magnitudes or relation reduction of the stall/lift-break coefficient.

NACA 23012 Wing

Because aircraft icing involves wings (and not airfoils), it was felt important to consider whether the preceding ice-shape location effect trends are also found for a typical wing configuration. A tapered NACA 23012 wing was therefore studied with a typical geometry of an aspect ratio of 5 and a taper ratio of 2, and with a Mach number of 0.12 with root Reynolds number of 10.5×10^6. For the ice location variation a quarter-round ice shape was attached at $x/c = 0.02$, 0.10, and 0.20, with the local ice-shape size fixed over the entire span as $k/c = 1.39\%$, that is, the ice-shape size was tapered from the root plane to the tip.

Figure 14a shows the lift curve for the iced wing and its comparison to the airfoil results with the ice shape located at 10% chord length. As expected, a slightly lower lift-curve slope is predicted for the wing compared with the airfoil (caused by finite-span losses), and the stall is slightly delayed for the wing. Also, the three dimensionality produced a stronger break in the lift-curve slope, nearly yielding a definitive $C_{l,\max}$. The simulated drag coefficient (Fig. 14b) for the wing is slightly lower than that of the airfoils, but in general the dimensionality had little effect on the drag.

Figure 14c shows the lift curve for the clean and iced wings. As predicted in the two-dimensional simulations, no obvious $C_{L,\max}$ and α_{stall} were predicted for the wings with ice shapes at $x/c = 0.10$ and 0.20, though the $x/c = 0.02$ did yield a maximum lift coefficient. With comparison to the lift-break value, the same critical ice-shape location $x/c = 0.10$ found in the airfoil study was also found for the wing, though its overall degradation was stronger for the wing (compare Figs. 9c and 14c), that is, a $C_{L,\text{break}} = 0.34$ vs a $C_{l,\text{break}} = 0.38$. This suggests that critical ice-shape location trends found for two-dimensional airfoils can be qualitatively (but not quantitatively) extended to wings at similar conditions. It can also be noted in Fig. 14d that the iced-wing drag values are much greater than the clean-wing drag value (similar qualitatively and quantitatively to the result found for the airfoil in Fig. 9d). As such, the large drag increase caused by the ice-shape presence overshadows the increase in induced drag as a result of finite span effects.

Conclusions

A Reynolds-averaged Navier–Stokes (RANS) methodology was applied in this study to investigate the ice-shape effect on airfoil and wing aerodynamics under diverse conditions. For clean airfoils the effect of increasing Reynolds number (for fixed Mach number) was to slightly increase the maximum lift coefficient, lift-curve slope, and pitching moment as well as to slightly decrease the drag coefficient. This trend was found to be consistent with experimental results. Increasing Mach number (for fixed Reynolds number) somewhat reduced the angle of attack at which stall occurred (and hence reduced the maximum lift coefficient) and also yielded larger drag coefficients and pitching-moment coefficients. For upper-surface iced airfoils the variations between Reynolds numbers were effectively negligible for both the experimental and computational results, and effect of Mach number was also minor.

With respect to upper-surface, ice-shape size on the NACA 23012 airfoil, a nearly two-fold increase in height does not lead to a commensurate reduction in lift coefficient, that is, the change is nonlinear with respect to ice-shape size. For the leading-edge iced NLF 0414 airfoil the size effect at the leading edge is still significant but not as large, and in general the variations in lift, drag, and pitching moment tend to vary more linearly with ice-shape size.

With respect to ice-shape location on the NACA 23012 airfoil, the maximum lift coefficient and stall angle of attack are lowest at the critical ice-shape location of $x/c = 0.10$. A similar result was noted for a NACA 23012 wing. However, because larger ice-shape heights tend to be found (in experimental accretion studies) near the leading edge as compared to along the upper surface it might be important to consider the critical position in the context of the likely ice-shape size for given chordwise locations (rather than only examining location sensitivity for a fixed ice-shape size).

The study for ice accretions on different airfoil models shows that the critical ice location varies with airfoil geometry, and in general the location tends to be in the neighborhood of (and sometimes in between) the positions of the maximum pressure gradient and the minimum pressure of the clean airfoil condition. However, an increase in the suction peak magnitude for a given lift coefficient for the clean airfoil condition does not generally corresponded to larger performance degradation under iced conditions.

With respect to overall fidelity, the RANS method shows reasonable prediction of the clean airfoil performance and of the iced airfoil aerodynamics up to stall conditions. However, the stall or poststall predictions were often unsatisfactory, particularly for the largest ice shapes and for ice shapes near the critical ice-shape location. This problem was alleviated to some degree by defining a lift-break coefficient and angle of attack, which both compared reasonably well with experimental stall values. This lack of quantitative fidelity for poststall behavior was attributed to the highly unsteady three-dimensional nature at the massively separated flows associated with large ice shapes at the critical location. To obtain a more robust computational capability for iced airfoil aerodynamics, vortex-capturing Navier–Stokes simulation methodologies (such as detached-eddy simulations or large-eddy simulations) should be considered.

Acknowledgments

This work was supported by the Federal Aviation Administration (FAA) under Grant DTFA MB96-6-023 with James Riley as Technical Monitor. The computations were performed with the support from National Center for Supercomputing Applications and UIUC Turing Linux Cluster Systems. The authors gratefully acknowledge the assistance of Gene Addy, Tom Bond, Michael Bragg, Andy Broeren, Satish Kumar, Sam Lee, Han Kim and Mark Potapczuk.

References

[1]Bragg, M. B., "Aircraft Aerodynamic Effects due to Large Droplet Ice Accretion," AIAA Paper 96-0932, Jan. 1996.

[2]Lee, S., and Bragg, M. B., "Experimental Investigation of Simulated Large-Droplet Ice Shapes on Airfoil Aerodynamics," *Journal of Aircraft*, Vol. 36, No. 5, 1999, pp. 844–850.

[3]Kim, H. S., and Bragg, M. B., "Effect of Leading-Edge Ice Accretion Geometry on Airfoil Aerodynamics," AIAA Paper 99-3150, Jan. 1999.

[4]Broeren, A., and Bragg, M. B., "Effect of Airfoil Geometry on Performance with Simulated Ice Accretions," Federal Aviation Administration, Vol. I—Experimental Investigation, Rept., Jan. 2003.

[5]Dunn, T., Loth, E., and Bragg, M. B., "Computational Investigation of Simulated Large-Droplet Ice Shapes on Airfoil Aerodynamics," *Journal of Aircraft*, Vol. 36, No. 5, 1999, pp. 836–843.

[6]Kumar, S., and Loth, E., "Aerodynamic Simulations of Airfoils with Upper-Surface Ice-Shapes," *Journal of Aircraft*, Vol. 38, No. 2, 2001, pp. 285–295.

[7]Potapczuk, M., "Numerical Analysis of a NACA 0012 Airfoil with Leading Edge Ice Accretions," AIAA Paper 87-0101, Jan. 1987.

[8]Chung, J. C. Y., Reehorst, A., Potapczuk, M., and Slater, J., "Navier–Stokes Analysis of the Flowfield Characteristics of an Ice Contaminated Aircraft Wing," AIAA Paper 99-0375, 1999.

[9]Kwon, O., and Sankar, O., "Numerical Study of the Effects of Icing on Finite Wing Aerodynamics," AIAA Paper 92-0757, Jan. 1990.

[10]Pan, J., and Loth, E., "Effect of Airfoil Geometry on Performance with Simulated Ice Accretions," Federal Aviation Administration, Vol. II—Numerical Investigation, Rept., Federal Aviation Administration at Atlantic City, NJ, Jan. 2003.

[11]Bush, R. H., Power, G. D., and Towne, C. E., "WIND: The Production Flow Solver of the NPARC Alliance," AIAA Paper 98-0935, Jan. 1998.

[12]Drela, M., and Giles, M. B., "Viscous-Inviscid Analysis of Transonic and Low Reynolds Number Airfoils," *AIAA Journal*, Vol. 25, No. 10, 1987, pp. 1347–1355.

[13]Pointwise, Inc., Gridgen User Manual, Bedford, TX, Ver. 14, May 2002.

[14]Gurbacki, H., and Bragg, M. B., "Sensing Aircraft Icing Effects by Unsteady Flap Hinge-Moment Measurement," *Journal of Aircraft*, Vol. 38, No. 3, 2001, pp. 575–577.

[15]Bragg, M. B., and Khodadoust, A., "Effect of Simulated Glaze Ice on a Rectangular Wing," AIAA Paper 89-0750, Jan. 1989.